Light Metals 2013 *Edited by: Barry Sadler*
TMS (The Minerals, Metals & Materials Society), 2013

EFFECTS OF Yb ADDITIONS ON REFINEMENT OF EUTECTIC Si IN Al-5Si ALLOYS

J.H. Li[1,*], P. Schumacher[1, 2]

[1*] Chair of Casting Research, Department of Metallurgy, the University of Leoben, A-8700, Leoben, Austria (jie-hua.li@hotmail.com)
[2] Austrian Foundry Research Institute, Parkstrasse 21, Leoben, Styria, A-8700, Austria

Keywords: Al-Si alloy; Yb additions; Refinement; Eutectic solidification; TEM.

Abstract

Modification of eutectic Si from platelet to fibrous morphology can be interpreted using impurity-induced twinning (IIT) growth mechanism and twin plane re-entrant edge (TPRE) growth mechanism. According to IIT mechanism, Yb has an exactly fitting radius ratio (1.646). However, to date, the effects of Yb additions on eutectic Si is still very limited. In this contribution, a series of Al-5 wt% Si alloys with Yb additions have been investigated using thermal analysis and multi-scale microstructure characterization techniques. Only a refined plate-like eutectic Si structure was observed. However, in contrast to Sr additions, no fibrous morphology and no significant Si twinning was observed, which is not consistent with the generally accepted IIT mechanisms. We proposed that the morphology change from platelet to fibrous, caused by stronger Si twinning, can be defined as modification; while, the decrease in size, caused by higher nucleation and growth undercooling, should be defined as refinement.

Introduction

Al-Si based alloys, i.e. A356, are dominant for the foundry application which constitutes the majority of all castings. The size and shape of eutectic Si in hypoeutectic Al-Si alloys and primary Si in hypereutectic Al-Si alloys has a key influence on the final mechanical properties of the manufactured parts. The modification of the Si morphology from flake-like to fibrous form greatly improves the mechanical properties. Therefore, the modification of eutectic Si in Al-Si alloys has been widely investigated in the field of solidification since the first modification phenomenon was discovered by Pacz in 1920 [1], where an Al-15 wt. % Si alloy was stirred in a sodium fluoride flux and a remarkable increase in the mechanical properties was achieved.

The modification of the eutectic Si in hypoeutectic Al-Si alloys is normally achieved in two different ways: by addition of certain modified elements (chemical modification) [2-13] or by rapid solidification (quench modification) [13], although ultrasonic vibration [14] and electromagnetic field [15] were also reported to refine the eutectic Si. With respect to chemical modification, several common modifying elements, i.e. Sr and Na, have been widely investigated over the years and are widely used in the casting industry to modify the Si morphology from flake-like to fine fibrous. However, the exact mechanism involved behind this process is still under debate. With respect to quench modification, our recent melt spun experiments [13, 17] clearly reveal that nano-scale twinned Si particles were formed directly from the liquid in Al-5 wt. % Si alloys with and without a trace modified elements (Sr and P) during rapid quenching. The addition of Sr (100 ppm) into Al-5Si based alloys was found to promote the twinning of Si particles on the grain boundary and the formation of Si precipitates in the α-Al matrix.

Although the modification mechanism is still a matter of debate, in particular nucleation, it was generally accepted that nucleation and growth mainly control modification. The impurity-induced twinning (IIT) growth mechanism proposed by Lu and Hellawell [2] and twin plane re-entrant edge growth mechanism (TPRE) proposed by Wanger [18] and Hamilton [19] are to date the accepted models. TPRE growth mechanism proposed that growth occurred more readily at the re-entrant corners during modification of Ge crystals. IIT growth mechanism proposed the impurities were adsorbed on the growing surfaces of Si and caused frequent twinning to occur. The geometrical, ideal radius ratio ($r_{modifier}/r_{Si}$) to cause IIT is about 1.646. Both IIT and TPRE mechanism have been experimental supported in the cases of Sr [9] and Eu [11]. However, only in the cases of Sr, twinning was observed by TEM under conventional casting condition with slow cooling rate. Eu and Sr have been observed to be present in the eutectic Si of Al-Si alloys using μ-XRF mapping [10, 11], STEM-EDX map and atom probe tomography [9], respectively, although μ-XRF mapping reveals that Sr is homogenously distributed within the eutectic Si, while STEM-EDX map and atom probe tomography shows Sr is segregated at the re-entrant corners and growing plane. This difference may be due to the techniques and resolution used, however, the segregation of Sr and Eu into eutectic Si indeed causes a fine fibrous morphology. A similar observation using electron probe microanalysis technique (EPMA) also shows that Sr resides mostly inside the Si in A356 alloy [12].

In contrast to Sr and Eu, Yb was not chemically detected to be present in the eutectic Si, but appeared to be precipitated independently in the vicinity to the Si phase [11]. This is remarkable as Yb has a suitable radius ratio of r_{Yb}/r_{Si}=1.646 exactly fitting the IIT theory. Moreover, previous work [8] suggests that the modification ability of an element may be the result of a certain combination of the valence electron charge number, the atom number and atomic radius of the modifier, also implying that Yb may be an effective modifier. However, to date, there are still only a limited number of detailed investigations on the effect of Yb addition on the eutectic Si phase in Al-Si alloys [4, 5, 11]. Particular pertinent questions that remain to be explored are (1) the distribution of Yb at the re-entrant edges/or corner of the Si crystal, (2) the effect of Yb on Si twining. The main motivation of this study is to investigate the effect of Yb addition at different levels on the eutectic Si phase in Al-5 wt. % Si alloys, with a focus on the distribution of Yb within Si and its effect on Si twinning.

Experimental material and procedures

A series of Al-5 wt. % Si alloys (wt. %, used though the paper unless otherwise noted) with Yb additions (up to 6100 ppm) were prepared using a commercial purity Al (99.7), Al-12Si (containing 0.9 Fe and 0.355 Mn) master alloy and Al-5Yb master alloy. For comparison, a high purity Al-5Si-6100 ppm Yb alloy was also prepared using a high purity Al (4N), Si (5N) and commercial purity Al-5Yb master alloy. The chemical concentration of Yb was determined by inductively coupled plasma atomic emission spectrum (ICP-AES) apparatus, while other elements are given as nominal composition in Table I.

Table I The chemical compositions of Al-5Si alloys with and without the Yb addition. (wt. %)

Alloy	Si	Fe	Mn	Yb (ppm)	Al
Alloy A	5.00	0.37	0.11	-	Balance
Alloy B	5.00	0.37	0.11	50	Balance
Alloy C	5.00	0.37	0.11	500	Balance
Alloy D	5.00	0.37	0.11	1000	Balance
Alloy E	5.00	0.37	0.11	2000	Balance
Alloy F	5.00	0.37	0.11	6100	Balance
Alloy G	5.00	-	-	6100	Balance

The experimental alloys were melted in an electric resistance furnace and the temperature of the melt was kept at 993 K. The Al-5Yb master alloy was added prior to casting. Each addition level was performed into a single batch. No degassing was performed prior to casting. At least two samples for each addition level were taken to perform thermal analysis using a quick-cup method. About 5 min after the Al-5Yb master alloy was added, thermal analysis was performed to elucidate the thermal kinetics during solidification.

Optical microscopy (OM), SEM and TEM were employed to characterise the microstructure. Samples for the optical microscopy, SEM and TEM observations were taken from the centre parts at the vicinity of the thermal couple. The specimens for OM and SEM investigation were mechanically ground, polished and then etched using a mixture of 13 g boric acid, 35 g HF, 800 ml H_2O. The specimens for TEM investigation were mechanically ground, polished and dimpled to about 30 μm, and then ion-beam milled using a Gatan Precision Ion Polishing System (PIPS, Gatan model 691). Transmission electron microscopy (TEM) was performed using a Philips CM12 microscopy operated at 120 kV and an image-side Cs-corrected JEOL-2100F operated at 200 kV.

Further investigation on the solidification behaviour was also performed by the Scheil simulation using Thermo-calc software with TTAL5 database, with the aim to predict the possible phases and their formation temperatures in the Al-5Si alloys with (Alloy A, commercial purity) and without (high purity) impurities. However, no similar simulation was performed for the other experimental alloys containing Yb (Alloys B to G) due to a lack of thermodynamic data.

Results

Thermal analysis of Al-5Si alloys with and without Yb additions

Figure 1 shows some typical cooling curves taken from Al-5Si alloys with and without the Yb addition. It should be noted that, for clarity, these cooling curves were separated (i.e. shifted by 100 s), respectively. The cooling rate during thermal analysis was evaluated to be about 22 K min^{-1}. The liquidus temperature of the Al-5Si based alloy (Alloy A) was evaluated to be about 903 K, as shown in Figure 1(b). With increasing Yb additions, the liquids of primary α-Al decreases (refer to the first peak of α-Al in Figure 1(d)). The decrease in the liquidus temperature with increasing Yb additions suggests that the ternary alloy behaves similar to the binary Al-Yb alloy. The eutectic arrest area is enlarged, as shown in Figure 1(c). The eutectic nucleation temperature (T_N), minimum temperature ($T_{Min.}$) and growth temperature (T_G) were determined and listed in Table II. For this purpose, the first derivative of the cooling curve was superimposed on the normal curve, as shown in Figure 1(d). The first derivative at each point represents the solidification rate of the alloy.

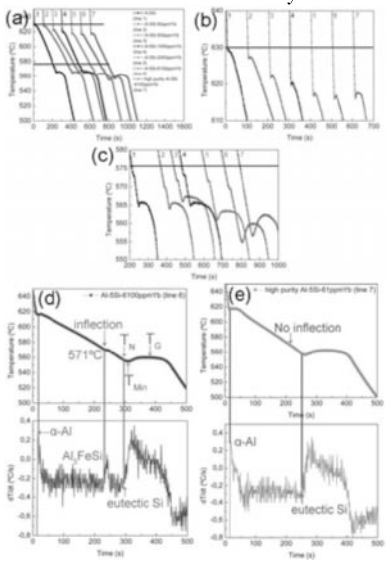

Figure 1. Cooling curves (a) taken from Al-5Si alloys with and without Yb addition. The nucleation of α-Al is enlarged in (b). The eutectic arrest area is also enlarged in (c). Special focus is on Alloy F (Al-5Si-6100 ppm Yb, line 6) (d) and Alloy G (high purity Al-5Si-6100 ppm Yb, line 7) (e). The main points (T_N, T_{Min}, T_G) are also marked in (d).

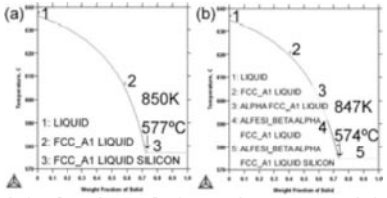

Figure 2. Weight fraction of phases in commercial purity Al-5Si alloy without (a) and with (b) Fe (0.37) and Mn (0.11) impurities, simulated by using scheil module with a database TTAL5.

The nucleation temperature, T_N, is defined as the point where the first silicon crystals nucleate and start to grow releasing latent heat. This is manifested by a change of slope in the cooling curve. This change in slope can be seen more clearly on the first derivative of the cooling curve [4]. The minimum temperature, T_{Min}, is defined as the point where the newly nucleated crystals, together with aluminium in the eutectic proportions, have grown

to such an extent that the latent heat, evolved during the growth process, balances the heat flow out of the system. This depends upon the cooling rate and heat capacity of the solidifying system. Furthermore, according to free growth model [20], free growth from particles stops at the T_{Min} because the critical radius becomes larger than the radius of the remaining inactive heterogeneous sites due to reheating. After this point, recalescence occurs, during which the release of latent heat surmounts the heat extraction from the system, a new heat balance is obtained, which rightfully should be defined as the "steady state growth temperature" of the eutectic reaction. Recalescence is the difference between the T_{Min} and T_G temperatures ($T_G - T_{Min}$).

Table II Nucleation temperature (T_N), minimum temperature (T_{Min}), growth temperature (T_G), nucleation undercooling (T_{eq}- T_N), growth undercooling (T_{eq}- T_G) and recalescence (T_G- T_{Min}) for Al-5Si alloys with and without the Yb addition.

Alloys	Nucleation undercooling T_{eq}- T_N (K)	Growth undercooling T_{eq}- T_G (K)	Recalescence T_G- T_{Min} (K)
Alloy A	0.0	8.4	1.1
Alloy B	0.9	7.6	1.7
Alloy C	0.5	6.6	1.4
Alloy D	1.3	9.5	2.1
Alloy E	2.9	10.5	2.7
Alloy F	3.8	14.0	5.4
Alloy G	18.2	14.7	5.8

The measured T_N of eutectic Si (i.e. 847 K for Alloy A without Yb addition) is close to the predicted equilibrium eutectic temperature (847 K) using Thermo Calc Scheil simulation with TTAL5 database, as shown in Figure 2(b), suggesting little or no undercooling. However, it should be noted that the nucleation temperature, T_N, is affected by the nucleation conditions in the alloys. Thermo Calc simulation only gives some information in equilibrium or Scheil condition. Nevertheless, Thermo Calc Scheil simulation indicates the impurity elements (Fe and Mn) depress the equilibrium eutectic temperature from 850 K to 847 K, as shown in Figure 2(a). The predicted eutectic temperatures (850 K and 847 K) were defined to be the equilibrium eutectic temperature (T_{eq}) of high purity Al-5Si alloy (Alloy G) and commercial purity Al-5Si alloys (Alloys A to F), respectively.

Up to 1000 ppm Yb addition, no great change of the thermal kinetics during solidification was observed. With increasing Yb addition, the eutectic arrest was displaced to lower temperatures (T_{Min}), suggesting that Si was hindered to grow by the Yb addition. The eutectic growth temperature (T_G) was also displaced to lower temperatures (i.e. 836.5 K, with 2000 ppm Yb addition, 833 K, with 6100 ppm Yb addition). In the case of high purity Al-5Si-6100 ppm Yb alloy (Alloy G), the eutectic growth temperature was also decreased to 835.3 K. It is worth noting that an inflection was observed for commercial purity alloys (Alloys A to F), as marked with a arrow in Figure 1(d), while no similar inflection was observed for high purity alloy (Alloy G), as shown in Figure 1(e). The formation of the inflection may be attributed to the impurity effects of Fe and Mn elements on nucleation and growth of eutectic Si, i.e. the formation of β-Al_5FeSi phase, as predicted in Figure 2(b).

The nucleation undercooling ($T_{eq} - T_N$) of the eutectic arrest was determined. No significant undercooling (0 K) was observed in the Alloy A without Yb addition. Increasing Yb addition results in increasing undercooling, suggesting deplete of possible nuclei (i.e. AlP) poisoned by Yb addition. It should be noted that a disagreement was also observed in Alloy B and Alloy C, which may be due to experimental error, however, the whole tendency is consistent. A higher undercooling (18.2 K) was observed for high purity Al-5Si-6100 ppm Yb alloy (Alloy G), much higher than 3.8 K for commercial purity Al-5Si-6100 ppm Yb alloy (Alloy F). This difference (14.4 K) can be attributed to even fewer nuclei (i.e. AlP) in the high purity Al-5Si-6100 ppm Yb alloy (Alloy G) which are poisoned by Yb addition. It should be noted that, in the case of high purity Al-5Si-6100 ppm Yb alloy (Alloy G), the eutectic nucleation temperature (T_N, 831.8 K) is slightly lower than the eutectic growth temperature (T_G, 835.3 K).

The same tendency is also true with the recalescence ($T_G - T_{Min}$) and growth undercooling ($T_{eq} - T_G$). A low recalescence (1.1 K) and growth undercooling (8.4 K) was observed in the Alloy A without Yb addition. No significant difference was observed with the Yb addition (up to 1000ppm). Increasing Yb addition (above 1000 ppm) results in increasing recalescence and growth undercooling. A relatively higher recalescence (5.8 K) and growth undercooling (14.7 K) was observed for high purity Al-5Si-6100 ppm Yb alloy (Alloy G), slightly higher than 5.4 K and 14.0 K for commercial purity Al-5Si-6100 ppm Yb alloy (Alloy F). This difference (0.4 K and 0.7 K) can be also attributed to the fewer nuclei (i.e. AlP), which almost require poisoning by Yb, in high purity alloys. On the basis of these results, the samples with the additions of above 1000 ppm Yb (Alloys D, E, F and G) were used for microstructure characterisation.

OM and SEM observation of Al-5Si alloys with and without Yb additions

Figure 3 shows representative eutectic structures observed by optical microscopy at low magnifications. For comparison, a high purity Al-5Si -200 ppm Na alloy is also shown in Figure 3(f). The eutectic Si in the alloy A without Yb addition is very coarse and flake-like, as shown in Figure 3(a). With the addition of up to 2000 ppm Yb (Figure 3(c)), the eutectic Si morphology remains unchanged, compared to the addition of 200 ppm Na. Up to 2000 ppm Yb, the eutectic Si is still plate-like, although a decrease in eutectic Si size was observed. A refined plate-like eutectic structure was achieved when the Yb content was increased to 6100 ppm (Figure 3(d)). It should be noted that, even in the case of 6100 ppm Yb addition, the eutectic structure is only refined in size, compared to the modification in shape and size of 200 ppm Na addition. The addition of high purity elements (Alloy G, Figure 3(e)) causes a more refined plate-like eutectic structure and no significant β-Al_5FeSi phase. The more refined plate-like eutectic structure of high purity alloy (Alloy G, Figure 3(e)) can be attributed to the relatively higher nucleation undercooling (18.2 K), growth undercooling (14.7 K) and recalescence (5.8 K) (Figure 1, Table II).

Overall distribution of Yb in the alloys can be easily observed by back scattered electron (BSE) image in SEM. The large atomic number difference makes compositional image possible, which gives rise to a brighter contrast of Yb containing phases in BSE image mode. Figure 4 shows an Yb containing phase observed in

Al-5Si-1000 ppm Yb alloy. Similar Yb containing phase was also observed above 1000 ppm Yb addition level (i.e., 2000 ppm Yb (Alloy E) and 6100 ppm Yb (Alloys F and G)). At 500 ppm Yb, the Yb containing phase was not observed, although it may also occur at this level. EDX analysis (Figure 4(b)) of the Yb containing phase, as marked in Figure 4(a), indicates that the Yb containing phase is the Al_2Si_2Yb phase. The Al_2Si_2Yb phase was also observed in high purity Al-5Si-6100 ppm Yb alloy (Alloy G), although the size and amount is less evident. No Yb was detected in the α-Al matrix using EDX, even up to 6100 ppm Yb addition.

In order to determine the crystal structure and lattice parameter of Al_2Si_2Yb phase using XRD analysis, a high purity Al-5Si-3Yb alloy was also prepared using the same method as for the other alloys. Back scattered electron (BSE) image and EDX analysis (not shown here) indicate that, even with higher Yb addition, most of the observed intermetallic phases are still Al_2Si_2Yb. XRD result (Figure 5) shows there are some strong peaks obtained from the Al_2Si_2Yb phase. The crystal structure and lattice parameters of the Al_2Si_2Yb phase was determined to be hexagonal (a=0.414482 nm, c=0.68927 nm), which is very close to the previous report [21] using powder (hexagonal (a=0.4144 nm, c=0.6915 nm)) and that of the Al_2Si_2Sr phase (Hexagonal, a=0.4187 nm, c=0.7427 nm), although c (0.68927 nm) is a little smaller than that (0.7427 nm) of the Al_2Si_2Sr phase (Table III).

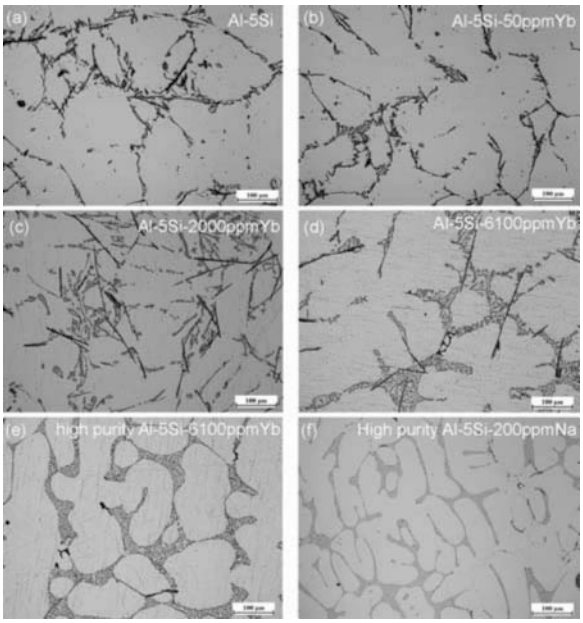

Figure 3. Representative eutectic structures observed by optical microscopy at low magnifications. (a) Al-5Si alloy, (b) Al-5Si-50 ppm Yb alloy, (c) Al-5Si-2000 ppm Yb alloy, (d) Al-5Si-6100 ppm Yb alloy, (e) high purity Al-5Si-6100 ppm Yb alloy. For comparison, a high purity Al-5Si -200 ppm Na alloy is also shown in (f).

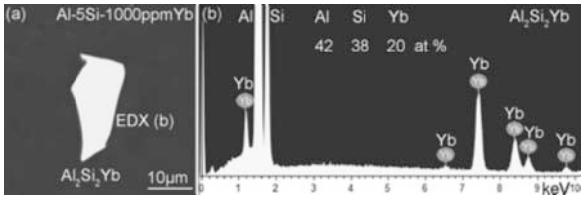

Figure 4. Back scattered electron image (a) and EDX analysis (b) of the Al_2Si_2Yb phase in Al-5Si-1000 ppm Yb alloy

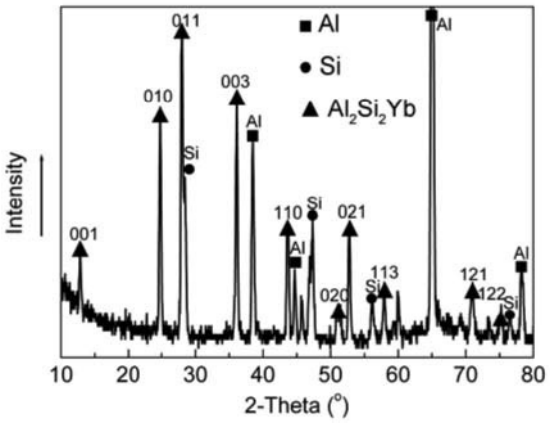

Figure 5. XRD analysis to determine the lattice parameter of Al_2Si_2Yb phase in high purity Al-5Si-3Yb alloy.

Table III Crystallographic data for some selected phases.

Phase	Crystal structure	Lattice parameter (nm)	Disregistry (δ) (%)
Al	Cubic	a= 0.40491	25 when $(Al)_S$
Si	Cubic	a= 0.5421	
Al_2Si_2Sr	Hexagonal	a= 0.41872, c= 0.7427	23 when $(Al_2Si_2Sr)_S$
Al_2Si_2Yb	Hexagonal	a=0.414482, c= 0.68927	23 when $Al_2Si_2Yb)_S$
AlP	Cubic	a= 0.5431	<1 when $(AlP)_S$
YbP	Cubic	a= 0.5554	<1 when $(YbP)_S$
$AlPO_4$	Hexagonal	a= 0.4390, c= 1.0940	19 when $(AlPO_4)_S$
Al_2O_3	Hexagonal	a= 0.4785, c= 1.2991	>19 when $(Al_2O_3)_S$

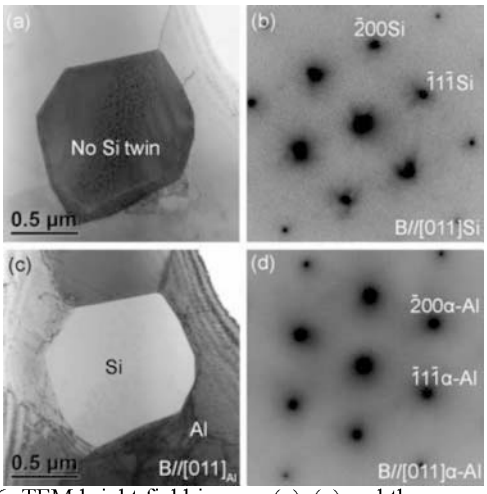

Figure 6. TEM bright field images (a), (c) and the corresponding SADPs (b), (d) of the factet Si phase on the grain boundary in commercial purity Al-5Si-6100 ppm Yb alloy. No clear Si twin was observed, although some surface artefact of oxidation on particles is present (a).

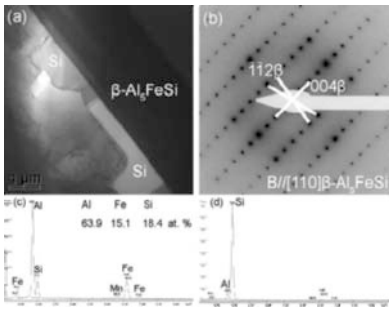

Figure 7. TEM bright field image (a) and corresponding SADP (b), EDX analyses (c, d) of the plate shaped Si phases in the vicinity of the β-Al_5FeSi phase in the commercial purity Al-5Si-6100 ppm Yb alloy.

Figure 8 shows another plate-like eutectic Si in the commercial purity Al-5Si-6100 ppm Yb alloy. The width of the plate-like Si is about 0.4 - 0.5 μm. Some round artefacts on the surface of Si phase are present; however, these artefacts are believed to form during TEM sample preparation. A grain boundary of Si phase ($\{111\}_{Si}$) and α-Al matrix ($\{123\}_{Al}$) was highlighted in Figure 8(b). Clearly, the cube to cube orientation relationship between the Si particles within α-Al matrix, which was often observed in high purity melt-spun Al-5Si alloy [13, 17], was not maintained at the grain boundary in this study. The TEM was set in nano-probe mode so that the investigated section was in the order of the electron probe itself. EDX analysis (Figure 8(c)) taken from the Si particle using a nanobeam (the beam size is about 1 nm) shows that only Si and Fe are present, while, Yb is not present. This indicates that Yb atoms do not concentrate in the eutectic Si, although Yb is present within the eutectic e.g. as Al_2Si_2Yb (Figure 4).

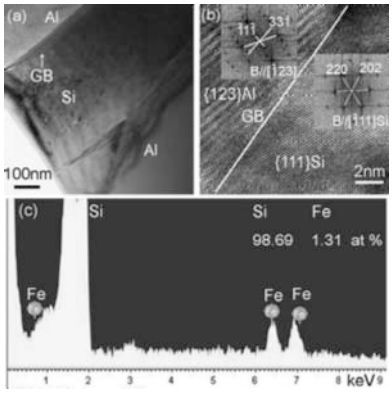

Figure 8. TEM bright field image of a plate shaped Si phase (a), high resolution TEM image of a grain boundary (b) in commercial purity Al-5Si-6100 ppm Yb alloy. (B// $<111>_{Si}$). EDX analysis (c) was taken from the Si particle.

An interesting question arises, where is the Yb located? Apart from the formation of large Al_2Si_2Yb phase (Figure 4), some small Yb containing precipitates were also observed in Al-Si eutectic in the commercial purity Al-5Si-6100 ppm Yb alloy, as shown in Figure 9(a). EDX analysis (Figure 9(c)) suggests the small Yb containing precipitate is also the Al_2Si_2Yb phase. The presence of Cu peak is due to the TEM holder. It is worth noting that the corresponding SADP (Figure 9(b)) was taken using a large aperture containing α-Al matrix, two Si particles and the Al_2Si_2Yb phase. However, no detailed structural information in form of orientation relationship between the phases could be obtained, although it has been observed previously [17].

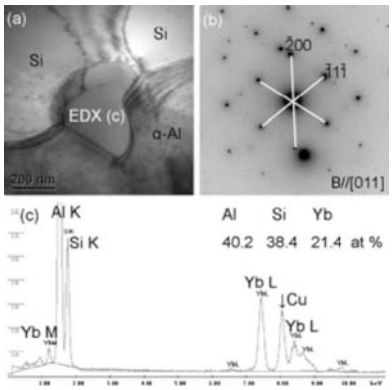

Figure 9. TEM bright field image (a) and corresponding SADP (b), EDX analysis (c) of the Al_2Si_2Yb phase in commercial purity Al-5Si-6100 ppm Yb alloy. The presence of Cu peak is due to the TEM holder.

Discussion

Refinement or modification of eutectic Si

A refined plate-like eutectic structure was achieved when the Yb content was increased to 6100 ppm (Figures 3(d) and (e)). Even with a higher Yb addition (up to 13400 ppm Yb in Al-10Si alloy, 10000 ppm Yb in Al-7.5Si-0.45Mg alloy) reported by other work [11], only refined Si can be achieved, compared to the modification of 200 ppm Na addition. Similar refinement of eutectic Si caused by the addition of other rare earth elements (i.e. Sc [6], La, Ce [7] et al) was also reported, and often regarded as modification [4, 5]. One particular question that arises is whether this "declared modification" caused by the addition of rare earth elements is equal to the modification caused by the addition of Sr and Na, showing significant twins in Si. It is generally accepted that modification of eutectic Si can be directly related to the depression of the eutectic growth temperature. In this study, a reduction of eutectic growth temperature (T_G, 836.5 K for 2000 ppm Yb addition (Alloy E), 833 K for 6100 ppm Yb addition (Alloy F)) was observed. However, only refined smaller Si was achieved. This strongly indicated that no direct relationship can be expected between the Si morphology and the depression of eutectic growth temperature. In contrast, growth undercooling ($T_{eq} - T_G$) and recalescence ($T_G - T_{Min}$) of the eutectic arrest shows a good prediction to the refinement effect of Yb addition. Lower growth undercooling (8.4 K for alloy A) and recalescence (1.1 K for alloy A) observed at Yb less than 2000 ppm, results in a very coarse and flake-like eutectic Si structure. Higher growth undercooling (14.0 K for alloy F and 14.7 K for alloy G) and recalescence (5.4 K for alloy F and 5.8 K for alloy G) leads to a refined plate-like eutectic structure. In this study, the formation of Al_2Si_2Yb phase (Figures 4 and 9) consumes most of Yb. Thus, increasing Yb addition results into a refined microstructure, especially for the high purity Al-5Si-6100 ppm Yb alloy (alloy G). Although, the recalescence (T_G - T_{min}) is also denoted as undercooling, however, undercooling is more commonly used to describe the drop of nucleation temperature (T_{eq}-T_N). As suggested by A.K. Dahle [5], the recalescence is also thought to be a good description of eutectic arrest.

The partitioning behaviour and the solute redistribution during solidification process are of great importance to elucidate the refinement or modification mechanism. Yb has a very limited solubility in Al. The maximum Yb solid-solubility in α-Al was measured by atom probe tomography to be 0.0248 ± 0.0007 (at. %) at 898 K [23]. The diffusivity of Yb in Al and the Al/Al_3Yb interfacial free energies at 573 K was also measured to be $(6 \pm 2) \times 10^{-17}$ m^2 s^{-1} and 0.6 ± 0.3 J m^{-2}, respectively [23]. During the solidification process, Yb and Si elements were rejected to the front of the advancing solid-liquid interface. An undercooling was established, as shown in Figure 1 and Table II, which restricts the growth of eutectic Si and thus refines the eutectic Si structure. This refinement mechanism caused by undercooling is different from the well-know IIT and TPRE modification mechanism, because, unlike Sr and Eu, Yb does not do not concentrate in the eutectic Si and show siginificant twins at conventional casting rate. Given the modification is mainly focused on the morphology change from plate-like to fibrous, we therefore, prefer to describe the effect of Yb as well as other similar rare earth elements (i.e. Y, Ce, Sc) on eutectic Si as a refinement, rather than a modification.

Last, but definitely not least, the cooling rate is also of great importance to the refinement or modification of eutectic Si. Higher cooing rate, such as chill casting and melting spinning in comparison to the sand casting, can extend the solid solubility of Yb in α-Al matrix [24], result in a solute redistribution of Yb, force twinning and thus a modification effect occurs. Further research on higher cooling rates is required to elucidate the effect of different cooling rates on refinement or modification of eutectic Si in Al-Si based alloys with Yb additions.

Conclusions

Thermal analysis and multi-scale microstructure characterization techniques have been employed to investigate the effect of Yb additions (up to 6100 ppm) on the eutectic Si in a series of Al-5 wt. % Si alloys. The following conclusions can be drawn:

(1) The addition of Yb was found to cause no modification effect to a fibrous morphology involving Si twining, however, a refined plate-like eutectic structure was observed.

(2) The Al_2Si_2Yb phase was observed above 1000 ppm Yb addition level. Within the eutectic Al and Si phase, the Al_2Si_2Yb phase was found as a precipitation from the remained liquid. No Yb was detected in the α-Al matrix or plate-like Si particle, even with up to 6100 ppm Yb addition. The absence of Yb element inside the eutectic Si may partly explain why no clear Si twinning was observed along $\{111\}_{Si}$ planes in the eutectic Si particles.

This investigation highlights to distinguish modifications in Al alloy. Here modification is defined as a transition from faceted to fibrous involving Si twining, while a reduction of the Si size is termed as refinement.

Acknowledgements

Jiehua Li gratefully acknowledges Prof Gerhard Dehm for his access to TEM and Prof Jozef Keckes for his help on XRD analysis at the Erich Schmid Institute of Materials Science of the Austrian Academy of Science.

References

[1] A. Pacz, U.S Patent No. 1387900, 1921.
[2] Shu-Zu Lu, and A.Hellawell, *Met. Trans. A*, 18 (1987), 1721-1733.
[3] B. Li, H.W. Wang, J.C. Jie and Z.J. Wei, *J. Alloys Compd.*, 509 (2011), 3387-3392.
[4] K. Nogita, A. Knuutinen, S.D. McDonald and A.K. Dahle, *J. Light Metal.*, 1 (2001), 219-228.
[5] A. Knuutinen, K. Nogita, S.D. McDonald and A.K. Dahle: *J. Light Mentals*, 1 (2001), 229-240.
[6] W. Prukkanon, N. Srisukhumbowornchai and C. Limmaneevichitr, *J. Alloys Compd.*, 477 (2009), 454-460.
[7] Y.C. Tsai, C.Y. Chou, R.R. Jeng, S.L. Lee and C.K. Lin, *Int. J. Cast Metal. Res.*, 24 (2011), 83-87.
[8] Q.Y. Zhang, C.G. Zheng and W.S. Han, *Acta Metall. Sin.*, 17 (1981), 130-136.
[9] M. Timpel, N. Wanderka, R. Schlesiger, T. Yamamoto, N. Lazarev, D. Isheim, G. Schmitz, S. Matsumura, and J. Banhart, *Acta Mater.*, 60 (2012), 3920-3928.
[10] K. Nogita, H. Yasuda, K. Yoshida, K. Uesugi, A. Takeuchi, Y. Suzuki and A.K. Dahle, *Scripta Mater.*, 55 (2006), 787-790.
[11] K. Nogita, H. Yasuda, M. Yoshiya, S.D. McDonald, K. Uesugi, A. Takeuchi and Y. Suzuki, *J. Alloys Compd.*, 489 (2010), 415-420.
[12] M. Faraji and L. Katgerman, *Micron.*, 41 (2010), 554-559.
[13] M. Zarif, B. McKay and P. Schumacher, *Metall. Mater. Trans. A.*, 42 (2011), 1684-1691.
[14] X. Jian, T.T. Meek and Q. Han, *Scripta Mater.*, 64 (2006), 893-896.
[15] J.B. Yu, Z.M. Ren and K. Deng, *Acta Metall. Sin.*, 24 (2011), 301-308.
[16] J.H. Li, M. Zarif, G. Dehm and P. Schumacher, *PHIL. Mag.*, DOI:10.1080/14786435.2012.687840.
[17] R.S. Wanger, *Acta Metall.*, 8 (1960), 57.
[18] R.D. Hamilton and R.G. Seidensticker, *J. Appl. Phys.*, 31 (1960), 1165.
[19] A. L. Greer, *Phil. Trans. R. Soc. Lond. A*, 361 (2003), 479-495.
[20] S. Bobev, P.H. Tobash, V. Fritsch, J.D. Thompson, M.F. Hundley, J.L. Sarrao and Z. Fisk, *J. Solid State Chem.*, 178 (2005), 2091–2103.
[21] L. Heusler and W. Schneider, *J. Light Metal.*, 2 (2002), 17-26.
[22] E. A. Brandes and C. J. Smithells, eds., Metals reference Handbook, 6th (London: Butterworths Publishing Company, 1983), 6-29.
[23] M. E. van Dalen, R.A. Karnesky, J.R. Cabotaje, D.C. Dunand and D.N. Seidman, *Acta Mater.*, 57 (2009), 4081-4089.
[24] Y.T. Ning, X.M. Zhou and H. Dai, *Acta Metall. Sin.*, 5 (1992), 327-333.